

# Ly $\alpha$ Leaks and Reionization

Longlong Feng<sup>1\*</sup>, Hongguang Bi<sup>1,2</sup>, Jiren Liu<sup>2</sup>, Li-Zhi Fang<sup>2</sup>

<sup>1</sup> *Purple Mountain Observatory, Nanjing, 210008, China*

<sup>2</sup> *Department of Physics, University of Arizona, Tucson, AZ 85721, USA*

## ABSTRACT

Ly $\alpha$  absorption spectra of QSOs at redshifts  $z \simeq 6$  show complete Gunn-Peterson absorption troughs (dark gaps) separated by tiny leaks. The dark gaps are from the intergalactic medium (IGM) where the density of neutral hydrogen are high enough to produce almost saturated absorptions, however, where the transmitted leaks come from is still unclear so far. We demonstrate that leaking can originate from the lowest density voids in the IGM as well as the ionized patches around ionizing sources using semi-analytical simulations. If leaks were produced in lowest density voids, the IGM might already be highly ionized, and the ionizing background should be almost uniform; in contrast, if leaks come from ionized patches, the neutral fraction of IGM would be still high, and the ionizing background is significantly inhomogeneous. Therefore, the origin of leaking is crucial to determining the epoch of inhomogeneous-to-uniform transition of the ionizing photon background. We show that the origin could be studied with the statistical features of leaks. Actually, Ly $\alpha$  leaks can be well defined and described by the equivalent width  $W$  and the full width of half area  $W_H$ , both of which are less contaminated by instrumental resolution and noise. It is found that the distribution of  $W$  and  $W_H$  of Ly $\alpha$  leaks are sensitive to the modeling of the ionizing background. We consider four representative models: uniform ionizing background (model 0), the photoionization rate of neutral hydrogen  $\Gamma_{\text{HI}}$  and the density of IGM are either linearly correlated (model I), or anti-correlated (model II), and  $\Gamma_{\text{HI}}$  is correlated with high density peaks containing ionizing sources (model III). Although all of these models can match to the mean and variance of the observed effective optical depth of the IGM at  $z \simeq 6$ , their distribution of  $W$  and  $W_H$  are very different from each other. Consequently, the leak statistics provides an effective tool to probe the evolutionary history of reionization at  $z \simeq 5 - 6.5$ . Similar statistics would also be applicable to the reionization of He II at  $z \simeq 3$

**Key words:** cosmology: theory - intergalactic medium - large-scale structure of the universe

## 1 INTRODUCTION

In the last decade, the Ly $\alpha$  forests of QSO's absorption spectra at redshifts  $z \leq 5$  have played an important role in understanding the diffuse cosmic baryon gas and the UV ionizing photon background, and constraining cosmological models and parameters (e.g. Rauch et al. 1997; Croft et al. 2002; Bolton et al. 2005; Seljak et al. 2005; Jena et al. 2005; Viel et al. 2006). Recently, more and more UV photon sources, including QSOs, GRB, Lyman-break galaxies, and Ly $\alpha$ -emitters at redshifts  $z > 5$  have been observed (see Ellis 2007 and reference therein). Due to the rapidly increase of Gunn-Peterson (GP) optical depth at  $z > 5$ , their absorp-

tion spectra show long dark gaps on scales of tens of Mpc separated by tiny transmitted leaks. It has been suggested that we are observing the end stage of reionization (Fan et al. 2006).

It has been known that the dark gaps are from the IGM where the density of neutral hydrogen are high enough to produce almost complete absorptions, however, where the transmitted leaks come from is still unclear. In photoionization equilibrium, the density of neutral hydrogen  $n_{\text{HI}} \propto \alpha \rho^2$ , here  $\alpha$  is the recombination rate and  $\rho$  is the density of IGM; therefore, even when most of the IGM are neutral enough to produce complete Ly $\alpha$  absorptions, it is still possible for the lowest density voids to provide prominent transmitted fluxes. On the other hand, the leaks can also come from ion-

\* E-mail: fengll@pmo.ac.cn

ized patches around ionizing sources where the intensity of UV radiation are higher than average.

The origin of leaking is crucial to understanding the history of reionization. According to commonly accepted scenario of the reionization, in the early stage, the ionized regions are isolated patches in the neutral hydrogen background (e.g., Ciardi et al. 2003; Sokasian et al. 2003; Mellema et al. 2006; Gnedin 2006; Trac & Cen 2006). and the subsequent growing and overlapping of the ionized patches lead to the ending of reionization (e.g., Ciardi et al. 2003; Sokasian et al. 2003; Mellema et al. 2006; Gnedin 2004). Thus, if leaks mostly come from ionized patches, reionization should happen in the early stage. In contrast, if they were produced in lowest density voids, the the UV ionizing background might has already underwent an evolution from highly inhomogeneous to uniform distribution.

A variety of statistics has been used to study the evolution of reionization, such as the mean and dispersion of GP optical depth, the probability distribution function (PDF) of the flux, and the size of dark gaps (e.g., Fan et al. 2002, 2006; Songaila & Cowie 2002; Paschos & Norman 2005; Kohler et al. 2007; Gallerani et al. 2006; Becker et al. 2006), but all of them seem to be ineffective to provide the information of leak's origin and the inhomogeneity of UV ionizing background. The GP optical depth is an average, and not sensitive to details of reionization. The statistical properties (mean and variance) of the GP optical depth at  $z \simeq 6$  can be well explained by either the fluctuation of ionizing background (Fan et al. 2006) or models with uniform ionizing background (Lidz et al. 2006; Liu et al. 2006, hereafter PaperI). The PDF of the flux is also insensitive to the geometry of reionization. In addition, the PDF is heavily contaminated by noise and distorted by resolution.

Dark gaps are defined to be continuous regions with optical depth above a threshold in spectra. Intuitively, the statistics of dark gap should contain the same information as leaks. However, the size of dark gaps are sensitive to the instrumental resolution, because higher resolution data contain more small leaks (e.g., Paschos & Norman 2005; PaperI), and they also are contaminated by observational noise. Moreover, dark gaps are from saturated absorptions, they are featureless and contains generally less information of non-saturated absorption.

In this paper we made a statistical approach to Ly $\alpha$  leaks. The purpose is to show that the statistical features of Ly $\alpha$  leaks would be effective tool to reveal the origin of Ly $\alpha$  leaks, and to probe the evolution of reionization. Similar to Ly $\alpha$  absorption lines, Ly $\alpha$  leaks have a rich set of statistical properties, such as the width of leak profile. Unlike dark gaps, the properties of Ly $\alpha$  leaks can be defined through integrated quantities, which are less contaminated by resolution and noise. Moreover, Ly $\alpha$  leaks are from regions of non-saturated absorptions and encode more information of reionization; therefore, the Ly $\alpha$  statistics would provide more underlying physics of reionization than all the above-mentioned statistics.

The paper is organized as follows. §2 describes the method to produce Ly $\alpha$  absorption samples. §3 presents the statistical properties of Ly $\alpha$  leaks with a uniform ionizing background. §4 analyzes the effect of inhomogeneous ionizing background. Conclusion and discussion are given in §5.

## 2 SIMULATION SAMPLES OF HIGH REDSHIFT LY $\alpha$ ABSORPTION SPECTRUM

### 2.1 Method

We simulate Lyman series absorption spectra of QSOs between  $z = 3.5$  and  $6.5$  using the same lognormal method as those for low redshifts  $z \simeq 2 - 3$  (e.g., Bi et al. 1995; Bi & Davidsen 1997). In this model, the density field  $\rho(\mathbf{x})$  of the IGM is given by an exponential mapping of the linear density field  $\delta_0(\mathbf{x})$  as

$$\rho(\mathbf{x}) = \bar{\rho}_0 \exp[\delta_0(\mathbf{x}) - \sigma_0^2/2], \quad (1)$$

where  $\sigma_0^2 = \langle \delta_0^2 \rangle$  is the variance of the linear density field on scale of the Jeans length. Obviously, the 1-point PDF of  $\rho(\mathbf{x})$  is lognormal. In this model, the velocity field of baryon gas is produced by considering the statistical relation between density and velocity field (Bi & Davidsen, 1997; Choudhury et al. 2001; Veil et al. 2002).

The dynamical bases of the lognormal model have gradually been settled in recent years. First, although the evolution of cosmic baryon fluid is governed by the Navier-Stokes equation, the dynamics of growth modes of the fluid can be sketched by a stochastic force driven Burgers' equation (Berera & Fang 1994). On the other hand, the lognormal field is found to be a good approximation of the solution of the Burgers' equation (Jones 1999). The one-point distribution of the cosmic density and velocity fields on nonlinear regime are consistent with lognormal distribution (e.g. Yang et al. 2001, Pando et al. 2002). Especially, it has been shown recently that the velocity and density fields of the baryon matter of the standard  $\Lambda$ CDM model is well described by the so-called She-L ev eque's universal scaling formula, which is given by a hierarchical process with log-Poisson probability distribution (He et al. 2006, Liu & Fang 2007).

The simulation is performed in the concordance  $\Lambda$ CDM cosmological model with parameters  $\Omega_m = 0.27$ ,  $h = 0.71$ ,  $\sigma_8 = 0.84$ , and  $\Omega_b = 0.044$ . The thermodynamic evolution in the IGM is actually a rather complex process, because the nonlinear clustering leads to a multi-phased IGM. As shown in cosmological hydrodynamic simulations (e.g., He et al. 2004), for a given mass density, the temperature of the IGM could have large scatters with differences up to two orders. Nevertheless, the equation of state in Ly $\alpha$  clouds can be well approximated by a polytropic relation with  $\gamma = 4/3$  (Hui & Gnedin; He et al. 2004). The neutral fraction  $f_{\text{HI}}$  is obtained by solving the photoionization equilibrium equation. The photoionization rate  $\Gamma_{\text{HI}}$  will be given in §2.2. We then construct synthetic absorption spectra by convoluting the neutral hydrogen density field with Voigt profiles. For each given  $z$ , the size of the simulation samples is  $\Delta z = 0.3$ , and there are  $2^{14}$  pixels in each simulation box.

### 2.2 Redshift-Dependence of Photoionization Rate

If the distribution of the IGM is uniform and the UV ionizing background is independent of redshift, the mean GP optical depth of Ly $\alpha$  absorption should approximately increase with redshift as  $(1+z)^{4.5}$ . The observations of dark gaps directly show that the GP optical depth undergoes a stronger evolution at  $z \simeq 6$ , and consequently, the UV ionizing background would decrease rapidly with redshift at  $z \simeq 6$ . The strong

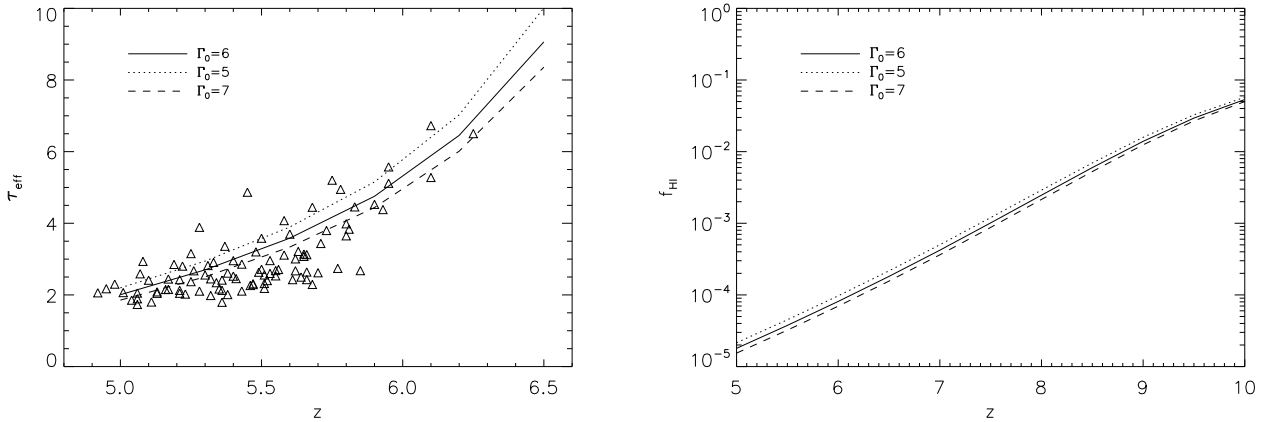


**Figure 1.** Redshift evolution of effective optical depth and neutral hydrogen fraction  $f_{\text{HI}}$  with the photoionization rate given by eq.(2). The amplitude is taken to be  $\Gamma_0 = 5, 6$  and  $7$ . The data points are taken from the Ly $\alpha$  observation of Fan et al. (2006).

evolution scenario of the UV ionizing background is supported by a number of simulations or semi-analytical models of reionization (e.g., Razoumov et al. 2002; Gnedin 2004; Oh & Furlanetto 2005; Pascho & Norman 2005; Wyithe & Loeb 2005; Kohler et al. 2007; Gallerani et al. 2006). It has been found that an evolution of photoionization rate as follows can fit the strong redshift evolution of the GP optical depth (Paper I) :

$$\Gamma_{\text{HI}}(z) = \Gamma_0 \exp\left\{-\left[\frac{1+z}{1+3.2}\right]^{2.4}\right\}, \quad (2)$$

which is in units of  $10^{-12} \text{ s}^{-1}$ . Note that the power index 2.4 in equation (2) is little different from the one used in Paper I because we use a different  $T_0$  in this paper (also see below).

With eq.(2), we calculate the redshift dependencies of neutral hydrogen fraction  $f_{\text{HI}}$  and the effective optical depth,  $\tau_{\text{eff}} \equiv -\ln(\bar{F})$ , where  $\bar{F}$  is the mean of transmitted flux. The results are plotted in Figure 1. The data points for  $\tau_{\text{eff}}$  are taken from Ly $\alpha$  observations of Fan et al. (2006). For best fitting, the amplitude  $\Gamma_0$  is in the range 5-7, which can be considered as the allowed range of  $\Gamma_{\text{HI}}(z)$ . In this paper, we will use  $\Gamma_0 = 6$  as the fiducial photoionization rate. It is interesting to note that  $f_{\text{HI}}$  approaches to  $\simeq 0.1$  at redshift  $z \simeq 10$ , which is consistent with the electron scattering optical depth given by the data of CMB polarization of WMAP III (Page et al. 2007).

It should be pointed out that the assumption of  $T_0 = 2 \times 10^4 \text{ K}$  (§2.1) is well reasonable at  $z \leq 5$  (e.g. Hui & Gnedin 1997; He et al 2004) and may still be applicable at  $z \simeq 6$  if the mass averaged neutral fraction of hydrogen is not larger than  $10^{-3}$ , and the photon heating rate is small. However, at higher redshift, say  $z \geq 6$ , the temperature  $T_0$  might be redshift-dependent. Yet, no proper information on  $T_0(z)$  is available at high redshift, and this leads to uncertainty of the model. Fortunately, in photoionization equilibrium, the neutral fraction  $f_{\text{HI}}$  depends mainly on a degenerate factor  $\Gamma_{\text{HI}}(z)T_0^{0.75}(z)$ . Thus, the problem with the uncertainty of  $T_0(z)$  can be overcome if we use the combined parameter of  $\Gamma_{\text{HI}}(z)[T_0(z)/2 \times 10^4]^{0.75}$  to fit the data. In the range  $z \leq 6$ , this parameter actually is  $\Gamma_{\text{HI}}(z)$ ; in the range of  $z > 6$ , it is different from  $\Gamma_{\text{HI}}(z)$  by a factor of  $[T_0(z)/2 \times 10^4]^{0.75}$ .

Thus, the redshift-evolution of  $\Gamma_{\text{HI}}(z)$  would be slower than eq.(2) if  $T_0(z)$  is less than  $2 \times 10^4 \text{ K}$  at higher redshifts.

### 2.3 An Example of Ly $\alpha$ Absorption Spectrum at $z = 6$

As an example of Ly $\alpha$  leaks, we plot a simulated sample of Ly $\alpha$  absorption spectrum at  $z = 6$  with a uniform ionizing background in Figure 2, which shows the transmitted flux  $F$ , the density  $\rho$  of baryon gas, the bulk velocity  $v$ , and the neutral hydrogen fraction  $f_{\text{HI}}$ . As expected, the mean of transmitted flux is very small, about 0.004, and corresponds to an effective optical depth 5.5. Nevertheless, we see spiky features with the transmitted flux  $F$  as large as 0.15. They are leaks.

At low redshifts  $z < 5$ , the Ly $\alpha$  forests in QSO's spectra have a spectral filling factor significantly less than one and can be decomposed into individual Ly $\alpha$  absorption lines. At redshifts  $z > 5$ , it is meaningless to decompose the spectra into individual lines since almost the whole spectra are absorbed completely. We note, however, the transmitted leaks look like emission features upon the dark background, and the absorption spectra can be decomposed into individual "emission lines", i.e., Ly $\alpha$  leaks.

Comparing the top, the second and bottom panels, we see that all the leaks comes from the regions with mass density less than 0.3 of the mean mass density of baryon gas. The neutral fraction for leaks is  $f_{\text{HI}} \sim 2 \times 10^{-5}$ , which yields a GP optical depth  $\sim 2.5$  for overdensity 0.25 and a  $F \sim 0.1$ , while the mean neutral fraction of the entire example is about  $7 \times 10^{-5}$ , which is high enough to produce dark gaps. The column density of neutral hydrogen of the leaking features is mainly in the range of  $10^{13}$ - $10^{14} \text{ cm}^{-2}$ , which are the non-saturated absorption regions, and therefore, leaks can come from regions where no enough neutral hydrogen to produce complete absorptions.

Similar to very high density clouds,  $\rho/\bar{\rho} \gg 1$ , the regions with very low density  $\rho/\bar{\rho} \ll 1$  are rare events in the cosmic clustering. Therefore, leaks may provide valuable test on models of clustering. For instance, the lognormal distributions are long tailed in both high and low density sides,

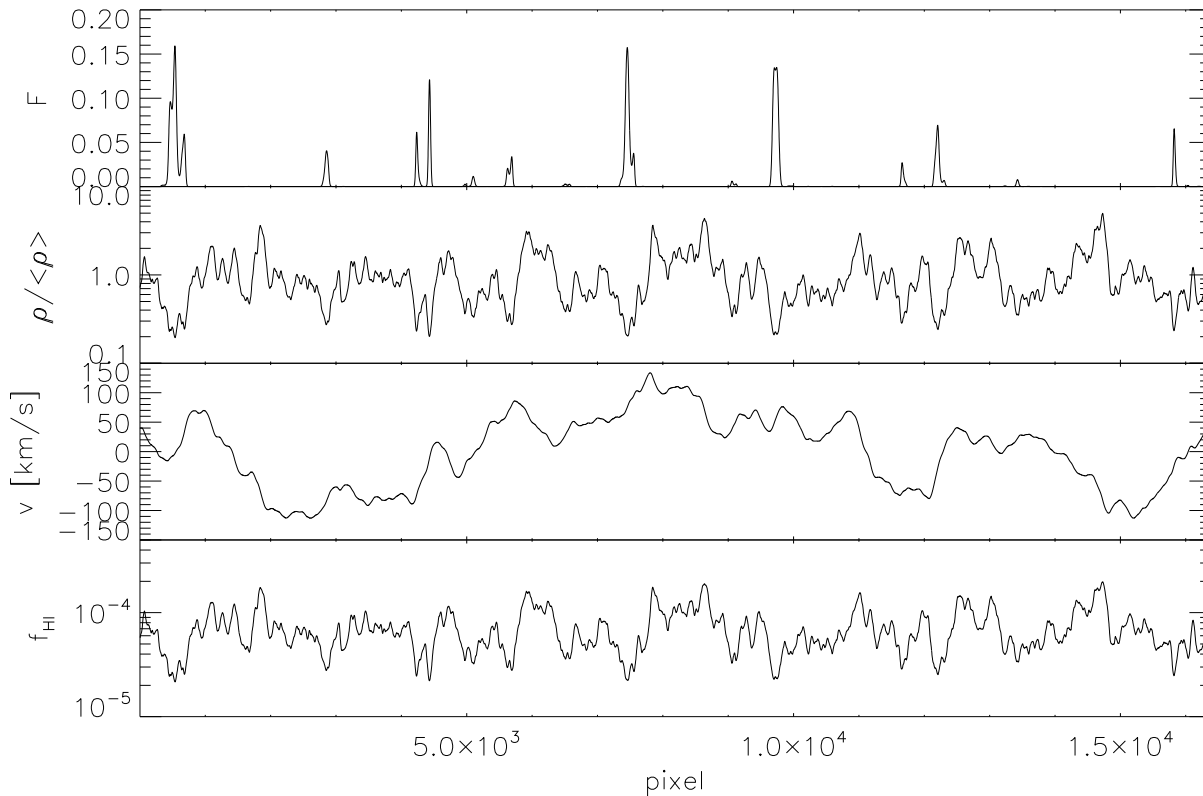


**Figure 2.** An example of simulated spectrum at  $z = 6$ . It shows the transmitted flux  $F$ , the density  $\rho$  of baryon gas, the velocity  $v$ , and the fraction of neutral hydrogen  $f_{\text{HI}}$  from top to bottom.  $\langle \rho \rangle$  is the mean of baryon matter.

and it contains more high density events as well as low density events than Gaussian model. It should be emphasized that, once the photoionization rate  $\Gamma_{\text{HI}}$  is determined from the GP optical depth, the statistical property of the sample shown in Figure 2 doesn't contain free parameters. These samples have been successfully used to explain the following observations: 1.) the large dispersion of the GP optical depth; 2.) the PDF of the flux, and 3.) the evolution of the size of dark gaps (Paper I). Now we use them to study the statistical properties of Ly $\alpha$  leaks.

### 3 STATISTICAL PROPERTIES OF LY $\alpha$ LEAKS

The Ly $\alpha$  absorption lines at low redshifts are described by well defined quantities, such as the equivalent width, FWHM (full width half maximum), and the Voigt profile, all of which are easily related to physical interpretations. Since the transmitted leaks look like emission features, one can decompose the spectra into individual "emission lines" and describes it by quantities similar to the Ly $\alpha$  absorption lines. In this section we study the statistical distribution of Ly $\alpha$  leaks in the model with a uniform ionizing background. The effects of inhomogeneous ionizing background will be discussed in next section.

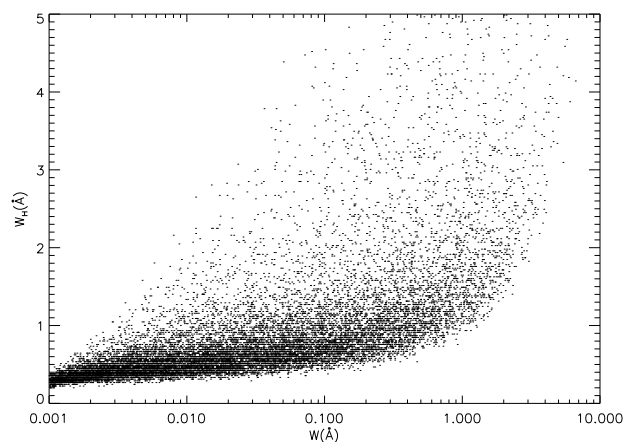


**Figure 3.** Relation between  $W$  and  $W_{\text{HI}}$  of Ly $\alpha$  leaks at  $z = 6$ .

#### 3.1 Profile of Leaks

The center of a leak is identified as the maximum of transmitted flux, and the boundaries are two nearby positions around the center where the flux falls down to zero or to noise level (we take it to be  $F = 0.001$  in this paper). The properties of leaks can be measured by two quantities: an equivalent width  $W$ , which is the total area under the pro-

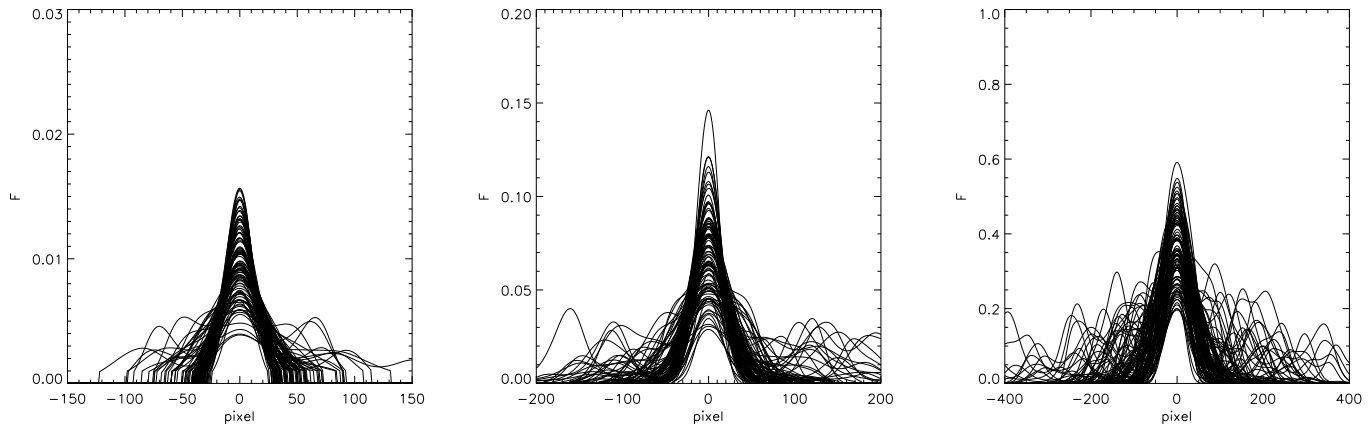


**Figure 4.** Profiles of leaks with equivalent widths  $W = 0.01$  (left),  $0.1$  (middle) and  $1 \text{ \AA}$  (right) of Ly $\alpha$  leaks at  $z = 6$ . One pixel is about  $0.022 \text{ \AA}$ .

file of a leak, and a half width  $W_H$ , which is defined as the width around center within which the area under the profile of the leak is equal to half of the total area of the leak.

The equivalent width  $W$  and the half width  $W_H$  are two independent measurements of Ly $\alpha$  leaks. This point can be seen in Figure 3, which gives the value of  $W$  and  $W_H$  for each leak at  $z = 6$ . It does not indicate a significant correlation between  $W$  and  $W_H$ , especially in the region of  $W > 0.1 \text{ \AA}$  and  $W_H > 0.1 \text{ \AA}$ . Figure 3 also shows that the distribution of  $W_H$  has a lower limit  $0.2 \text{ \AA}$ , which is due to the Jeans scale used for smoothing the sample. On the other hand, the equivalent width  $W$  distributes in the range from  $0.001 \text{ \AA}$  to  $5 \text{ \AA}$ . Obviously, one is unable to introduce two independent quantities for characterizing dark gaps.

The profiles of 100 randomly sampled leaks with  $W = 0.01, 0.1, \text{ and } 1 \text{ \AA}$  are displayed in Fig.4. The tails of the profiles in the three panels of Fig.4 look like the Lorentz profile, and of course, they do not have the meaning of the natural width of an absorption line. The profiles of leaks for a given equivalent width  $W$  have very large dispersions; for example, for  $W=0.1 \text{ \AA}$ , the flux covers a range from  $F = 0.03$  to  $0.15$ , and  $W_H$  can be  $0.4$  to  $4 \text{ \AA}$ . As the leaks are formed out of the two neighboring complete absorption troughs, which depend on inhomogeneities of density, velocity, and temperature fields, the large scatter of the profiles is expected.

Figure 4 also shows that some leaks may have multiple local maximums above the noise level. For clarity and easy-operating, we treat them as one leak. The current observational resolution is of the order of  $10 \text{ km/s}$ , which corresponds to  $\Delta\lambda \sim 0.28 \text{ \AA}$  in observer's frame, or about 13 pixels of simulation. Therefore, the observed Ly $\alpha$  leaks would have a resolvable width.

### 3.2 Number Density Distributions of Ly $\alpha$ Leaks

Similar to Ly $\alpha$  forests, we can define the cumulative number densities  $n(> W, z)$  and  $n(> W_H, z)$  of leaks as the number of leaks with widths larger than a given  $W$  and  $W_H$  at  $z$  per unit  $z$ , respectively. The differential number densities are  $n(W, z) = dn(> W, z)/dW$  and  $n(W_H, z) = dn(> W_H, z)/dW_H$ . It should be pointed out that statistics of  $W$  and  $W_H$  are not the same as the largest peak width

statistics proposed by Gallerani et al. (2007), which considered only the largest peak width. A peak may contain more than one leak, i.e. leak statistics describe the details of the leaking area. The mean transmitted flux at  $z$  within  $dz$  is  $\bar{F} = \int_0^\infty n(W, z) W dW$ . We calculate the number densities of leaks in redshift range  $z = 5 - 6.5$ . In each redshift region we produce 100 light-of-sight samples to calculate the density functions. The results are shown in Figure 5. The errors are estimated by Jackknife method, i.e., the variance over 5 subsamples, each of which contains 20 light-of-sight samples.

The number density  $n(W, z)$  shown in the up-left panel of Figure 5 are similar to a Schechter function: they follow a power law at small  $W$  and have a cut-off at large  $W$ . The distribution of  $n(W_H, z)$  at  $W_H < 0.5 \text{ \AA}$  declines with decreasing  $W_H$ , this is because of the Jeans length smoothing.

The slope of  $n(W, z)$  and  $n(W_H, z)$  are smaller for small redshift. It means the lack of low density voids with small size. That is, the increase of voids of small size is less than voids of large size. This trend can also be seen from the flattening of the cumulative density distributions  $n(> W_H, z)$  and  $n(> W, z)$ .

The redshift-evolution of the number densities  $n(> W, z)$  and  $n(> W_H, z)$  of leaks for  $W, W_H = 0.5, 1.0, \text{ and } 3.0 \text{ \AA}$  are shown in Figure 6. As has been seen in Figure 5, the number densities dramatically decrease at higher redshifts. The evolution is more rapidly for large leaks: the number density  $n(> W = 0.5 \text{ \AA}, z)$  drops by a factor of  $\sim 5$  when redshift increasing from 5 to 5.8, while  $n(> W = 3 \text{ \AA}, z)$  drops by a factor of  $\sim 60$ . The evolution trend is the same for the number density  $n(W_H, z)$ . From the error bars of Figures 5 and 6 we see that the predicted features of leaks would be able used to compare with observed data set containing 20 or more light-of-sight samples with the similar quality as simulation.

### 3.3 Effects of Resolution and Noise

In this section, we study the observational and instrumental effects on the statistics of leaks. Since both  $W$  and  $W_H$  are defined through the area under the profile of leaks, the effects of resolution and noise would be small. To simulate the

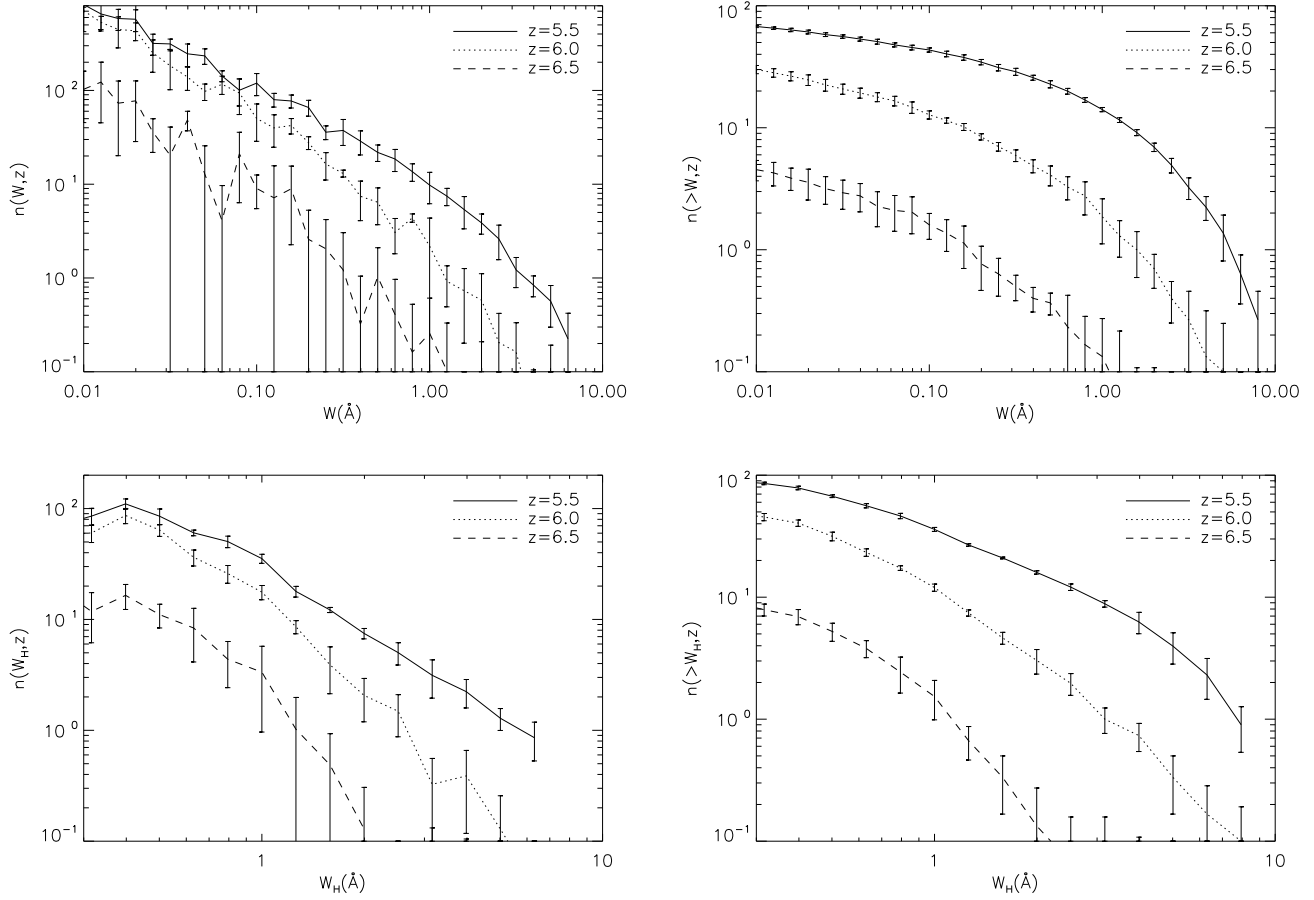


**Figure 5.** Number densities  $n(W, z)$ ,  $n(> W, z)$ ,  $n(W_H, z)$ , and  $n(> W_H, z)$  of leaks at redshift  $z = 5.5, 6.0$  and  $6.5$  from top to bottom. The error bars are the  $1\text{-}\sigma$  range given by Jackknife estimation, in which each subsample contains 20 lines of the absorption spectrum.

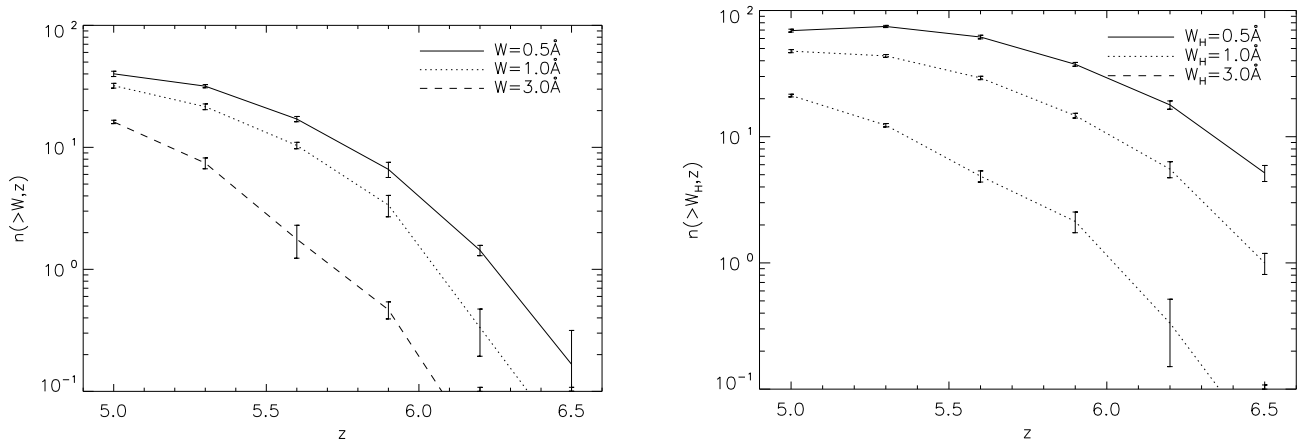


**Figure 6.** Redshift evolution of number densities  $n(> W, z)$ ,  $n(> W_H, z)$ ,  $n(W, z)$ , and  $n(W_H, z)$  of leaks with  $W, W_H = 0.5, 1.0$ , and  $3.0 \text{ \AA}$ . The error bars are the  $1\text{-}\sigma$  range given by Jackknife estimation, in which each subsample contains 20 lines of the absorption spectrum.

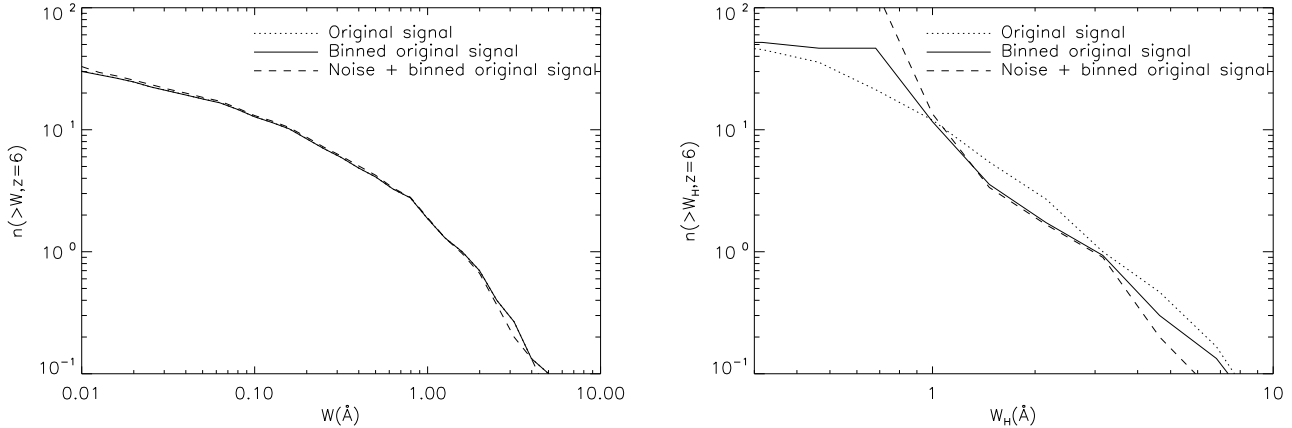


**Figure 7.** Effects of resolution and noise on number densities  $n(> W, z)$  (left panel) and  $n(> W_H, z)$  (right panel) for leaks at  $z = 6$ .

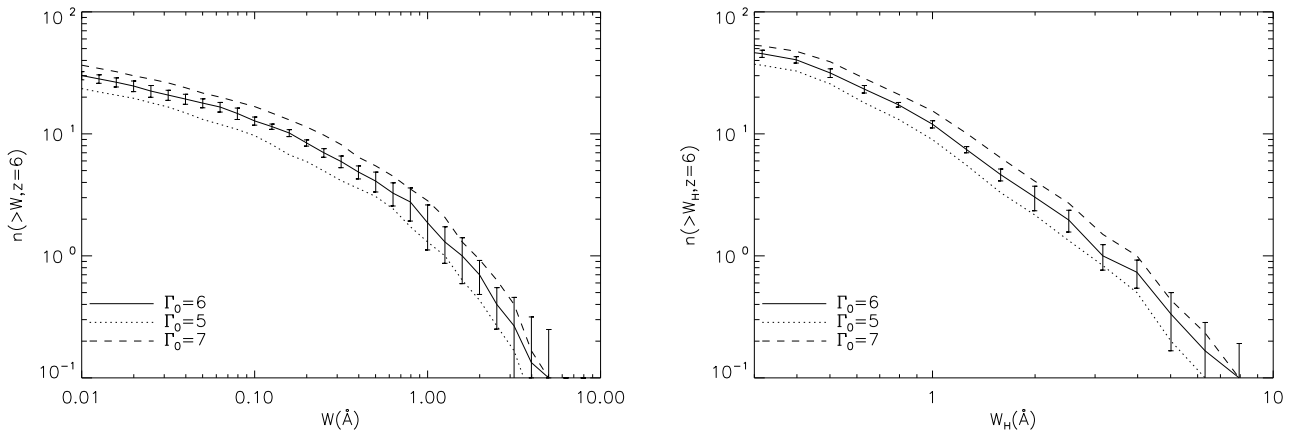


**Figure 8.** Number densities  $n(> W, z)$ , and  $n(> W_H, z)$  for samples at  $z = 6$  with  $\Gamma_0 = 5, 6, 7 \times 10^{-12} \text{ s}^{-1}$ , respectively. The error bars are the same as Figure 5.

observational effects, we bin the original data to a coarse grid corresponding to a resolution of 20000, and we add Gaussian noises with signal-to-noise ratio  $S/N=3$  on binned pixels. The number densities of leaks for the noisy binned samples are shown in Figures 7.

The effect of binning and noise is very small for  $W$ : the original plot of  $W$  actually is the same as the plot of binned  $W$ , and the distribution of noisy  $W$  is affected only when  $W < 0.01 \text{ \AA}$ . The effect of binning for  $W_H$  is also small on scales larger than the binning length. As expected, the noise effects for  $W_H$  are significant for  $W_H < 0.4 \text{ \AA}$ . The noise effects for  $W_H$  are even smaller if we smooth the noisy sample. This is very different from the PDF of the flux and the size of dark gaps, both of which are heavily contaminated by instrumental resolution and observational noises.

One can compare the uncertainty of  $\Gamma_0$  with the effect of noises. Figure 8 shows the number densities for the UV background amplitude  $\Gamma_0 = 5, 6, \text{ and } 7$  (eq.2), which represent the allowed range of  $\Gamma_0$ . Different from noises, the difference of  $\Gamma_0$  will cause uncertainty in the whole ranges of  $W$  and  $W_H$ . The uncertainties of number densities are within a factor of 2 when the amplitude  $\Gamma_0$  changes from

7 to 5. These uncertainties essentially are from the mass density perturbations with long wavelengths (Paper I). The error bars from the scattering of light-of-sight samples is also shown in Figure 8. Therefore, the scattering of  $\geq 20$  light-of-sight samples actually is less than the uncertainty of  $\Gamma_0$ .

#### 4 Ly $\alpha$ LEAKS OF INHOMOGENEOUS IONIZING BACKGROUND

In the early stage of reionization, ionizing photons are mainly in ionized patches around UV ionizing sources, and therefore, the spatial distribution of ionizing background is highly inhomogeneous and has patchy structures. When the ionized patches spread over the whole space, the ionizing background become uniform or quasi-uniform, and so the ionizing background underwent an inhomogeneous-to-uniform transition during the reionization. In this section we study the effects of inhomogeneous ionizing background on Ly $\alpha$  leak statistics.

#### 4.1 Models of Inhomogeneous Ionizing Background

The first question is how to model the inhomogeneous spatial distribution of the ionizing photon field. To our problem, the most important property is the relation between the fields of mass density and ionizing photon background or photoionization rate. If the spatial fluctuation of photoionization rate  $\Gamma_{\text{HI}}(\mathbf{x}, z)$  is statistically uncorrelated with the density field  $\rho(\mathbf{x}, z)$ , the reionization of IGM will statistically be the same as a uniform ionizing background, regardless of the details of the fluctuation of  $\Gamma_{\text{HI}}(\mathbf{x}, z)$ . In this case, the only effect of the fluctuations would be to yield a larger variance in relevant statistics. However, as shown in last sections, the uncertainty of the leak statistics is already large even when the ionizing background is uniform, and therefore, one would not be able to distinguish the fluctuating photon field from inhomogeneous density field if they are uncorrelated.

Although many simulations on the UV photon field at the epoch of reionization have been done, there still lack the results of the correlation between photon and density fields. In this context, we will consider the following four models on the statistical relation between the inhomogeneous fields of photon and density, which are mainly based on physical consideration of different stage of reionization.

*Model 0.* The photoionization rate is spatially uniform. It corresponds to the post-overlapping stage of reionization. This model has been used in last two sections.

*Model I.* The photoionization rate at a give redshift is assumed to be proportional to the density field of IGM,  $\Gamma_{\text{HI}} = \Gamma_{\text{I}}\rho$ ,  $\Gamma_{\text{I}}$  being a constant. This model is motivated by the so-called inside-out scenario: high density regions around UV sources are ionized first, and is most probable at the early stage of reionization.

*Model II.* Just opposite to model I, the photoionization rate at a give redshift is assumed to be inversely proportional to the density field of IGM,  $\Gamma_{\text{HI}} = \Gamma_{\text{II}}\rho^{-1}$ ,  $\Gamma_{\text{II}}$  being a constant. This model comes from the so-called outside-in scenario: under-dense regions are ionized first (Miralda-Escude et al. 2000), which is applicable at the late stage of reionization (Furlanetto & Oh 2005).

In order to fit the observed effective optical depth  $\tau_{\text{eff}}$  at redshift  $z = 6$ , we take the following parameters:  $\Gamma_{\text{I}} = \Gamma_0 \times 3.53$ ,  $\Gamma_{\text{II}} = \Gamma_0/2.77$  where  $\Gamma_0$  is the photoionization rate at  $z = 6$  for uniform ionizing background [eq.(2)].

*Model III or patch model.* This model corresponds to the stage before the overlapping of ionized patches. The IGM is almost fully neutral except for some isolated ionizing patches. We model the ionized patch as a Stromgren sphere: the neutral hydrogen fraction is equal to 0 within the patch and equal to 1 outside the patch. The mean radius of the Stromgren sphere is assumed to be  $R_s \simeq 1.8$  comoving Mpc, which corresponding to an UV photon source with luminosity  $L = 5 \times 10^{43}$  erg s $^{-1}$  with active time  $10^7$  year and a  $\nu^{-3}$  spectrum. To fit the observed optical depth, we found there should be 2 patches every simulated box ( $\Delta z = 0.3$ ). This number is actually consistent with the following estimation

$$\frac{dN}{dz} = \frac{\pi R_s^2 \phi(L) c}{H(z)}, \quad (3)$$

where  $\phi(L)$  the comoving luminosity function, i.e. the 3-D

number density of sources with luminosity  $L$ . Using  $\phi(5 \times 10^{43}) \sim 1.5 \times 10^{-3}$  Mpc $^{-3}$  (Bouwens et al. 2006), we have  $dN/dz \simeq 7$  and  $(dN/dz)\Delta z \simeq 2$ .

#### 4.2 Ly $\alpha$ Leaks of Inhomogeneous Ionizing Background

For the four models described in the last section, we recalculate the transmitted flux with the same underlying density and velocity fields of fig2. The results are shown in Figure 9. As mentioned above, the mean of transmitted flux for all models takes approximately the same value of 0.004, which corresponds to an effective optical depth  $\simeq 5.5$ . However, Figure 9 shows clearly different behaviors of Ly $\alpha$  leaks in various models.

For models I and II, the leaks appear exactly at the same positions as model 0 except some small leaks, which are more prominent for model I. In other words, all the leaks of models 0, I and II are from lowest density voids. Therefore, the three models have the same distribution of dark gaps, and it is impossible to discriminate among these models with the dark gap statistics.

However, the profiles of the leaks of model 0, I and II are statistically different from each other. For model I, the leaks generally have larger width and lower height than model 0, while for model II, the width of leaks generally is narrower than model 0, and the height of leaks is larger than model 0. The reason is straightforward. Comparing with model 0, model I gives a higher  $f_{\text{HI}}$  at low density and lower  $f_{\text{HI}}$  at high density. This leads to lower amplitude and broader width. For model II, the effect is just opposite to model I and yields higher amplitude and narrower width.

In the patch model, all the leaks come from ionized patches, within which ionizing sources are enclosed, and so the internal information of ionized patches can be inferred from the leak statistics. The size of dark gaps is actually given by the distance between ionized patches. Generally, Ly $\alpha$  leaks in the patch model have a maximum flux  $\simeq 0.6$ , which is higher than the maximum flux of other models, 0.2. This is because the neutral fraction within the Stromgren sphere is much less than other models. This behavior is similar to the so-called proximity effect of QSOs at low redshift (e.g., Rauch 1998). Thus, the statistics of the maximum flux of Ly $\alpha$  leaks may be used to reveal the patchy origin of Ly $\alpha$  leaks.

As we sample the size of patches along the sight of light according to the impact probability, the size of patches is smaller than  $R_s$ . If the size is too small, the ionized patch will be opaque to Ly $\alpha$  photons due to the damping wing of the surrounding neutral hydrogen absorption (Miralda-Escude 1998). Obviously, it explains why only one leak is apparent in the patch model as displayed in Figure 9.

#### 4.3 Number Densities of Ly $\alpha$ Leaks of Inhomogeneous Ionizing Background

We now calculate the number densities  $n(W, z)$ ,  $n(> W, z)$ ,  $n(W_{\text{H}}, z)$  and  $n(> W_{\text{H}}, z)$  for three inhomogeneous ionizing background models at  $z = 6$ , and the results are shown in Figures 10. We can see from Figure 10 that the effects of different models on the number densities of  $W$  and  $W_{\text{H}}$  are

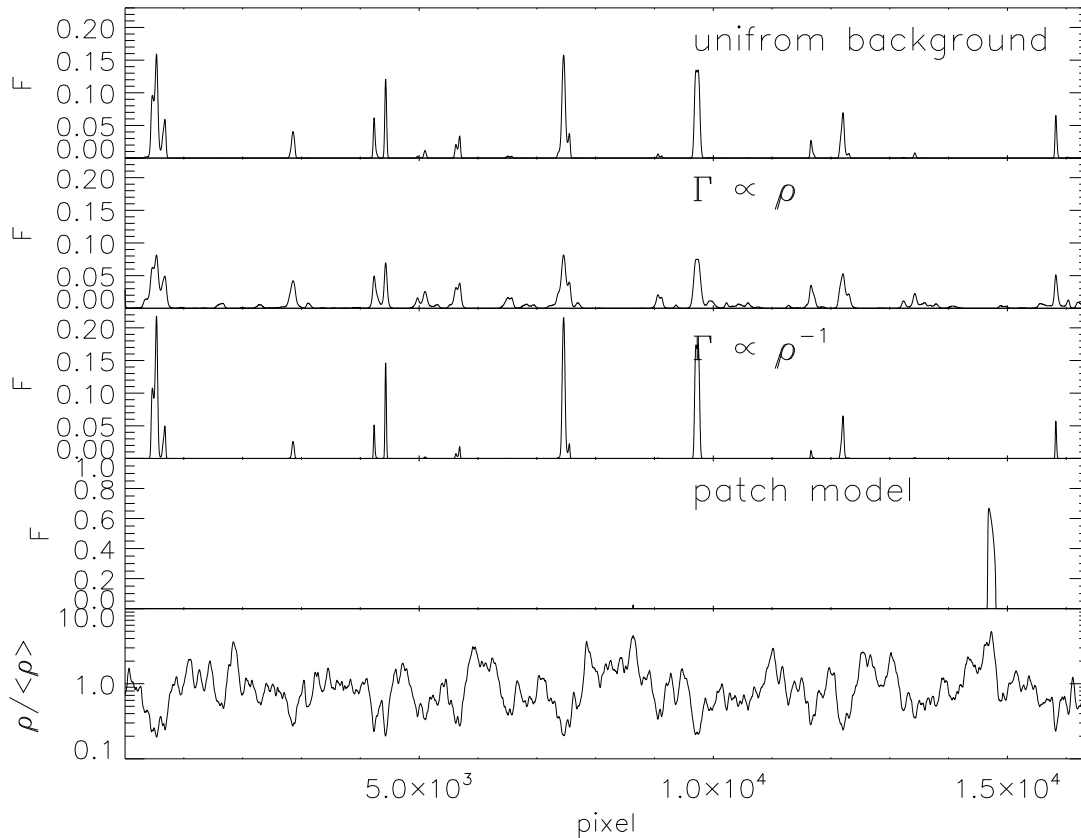


**Figure 9.** Transmitted flux  $F$  given by uniform ionizing background (top panel), the Model I (second panel), the Model II (third panel) and the Model III (fourth panel). The density field  $\rho$  of baryon gas (bottom panel) is the same as Figure 2.

different. That is, although all the models of 0, I, II and III give the same mean effective optical depth, their leak distributions are different. For clarifying, in Figures 10 we show only error bars for the curves of model 0. It would be enough to show that these results can be tested with data set containing about 20 light-of-sight data.

First, for model I, both of the number densities  $n(W, z)$  and  $n(> W, z)$  have only small deviations from model 0. However,  $n(W_H, z)$  are significantly different from their counterparts of model 0. The number density of leaks with  $W_H > 1 \text{ \AA}$  is much more than model 0. The basic feature of model I is to increase the number of leaks with large  $W_H$  as shown in Figure 9.

Second, for model II, we see once again that the number densities  $n(W, z)$  and  $n(> W, z)$  have only small deviations from model 0. Yet, the number densities  $n(W_H, z)$  and  $n(> W_H, z)$  of the model II are systematically lower than model 0. Therefore, the basic feature of model II is to keep the total area under the profile of leaks almost unchanged, but the widths of leaks are significantly narrowed.

Finally, the behavior of patch model is very different from models 0, I and II. As expected, the patch model yields more leaks with large  $W$ , and  $n(W, z)$  shows a bump around  $W = 3 - 5 \text{ \AA}$ , which characterize the area of the ionized patches. On the other hand, the number densities of  $n(W_H, z)$  and  $n(> W_H, z)$  are lower than model 0 because the characteristic size of ionized patches is less than that

of low density voids. It is interesting to note that for the patch model, the tails of  $n(W, z)$ ,  $n(> W, z)$  and  $n(W_H, z)$ ,  $n(> W_H, z)$  are quite different from each other. Generally, the tails of  $n(W, z)$  and  $n(> W, z)$  can extend to as large as  $W \simeq 5 \text{ \AA}$ , while for  $n(W_H, z)$  and  $n(> W_H, z)$ , there are no tails higher than  $3 \text{ \AA}$ . It results partially from the damping wing effect (Miralda-Escude 1998).

In summary, the statistical properties of leaks with respective to  $W$  and  $W_H$  are sensitive to the details of ionizing photon field. Combining the distribution of  $W$  and  $W_H$ , the Ly $\alpha$  leaks would be able to probe the origin of themselves, and thus reveal the ionization state of IGM, the inhomogeneity of ionizing background, and the evolution stage of reionization.

It should be pointed out that we considered only the patches of the HI regions around high redshift galaxies. The HI regions around quasars or the proximity effect would also be the patches of leaking. The mean luminosity of quasars probably is higher than galaxies, and therefore, the above-mentioned feature of  $n(W_H, z)$  and  $n(> W_H, z)$  would be more prominent for the patches of quasars. The damped Ly $\alpha$  absorption system is important for modeling low redshift Ly $\alpha$  absorption. Since these systems have high column density of neutral hydrogen, it will not contribute to leaking either in density void models or patch model.

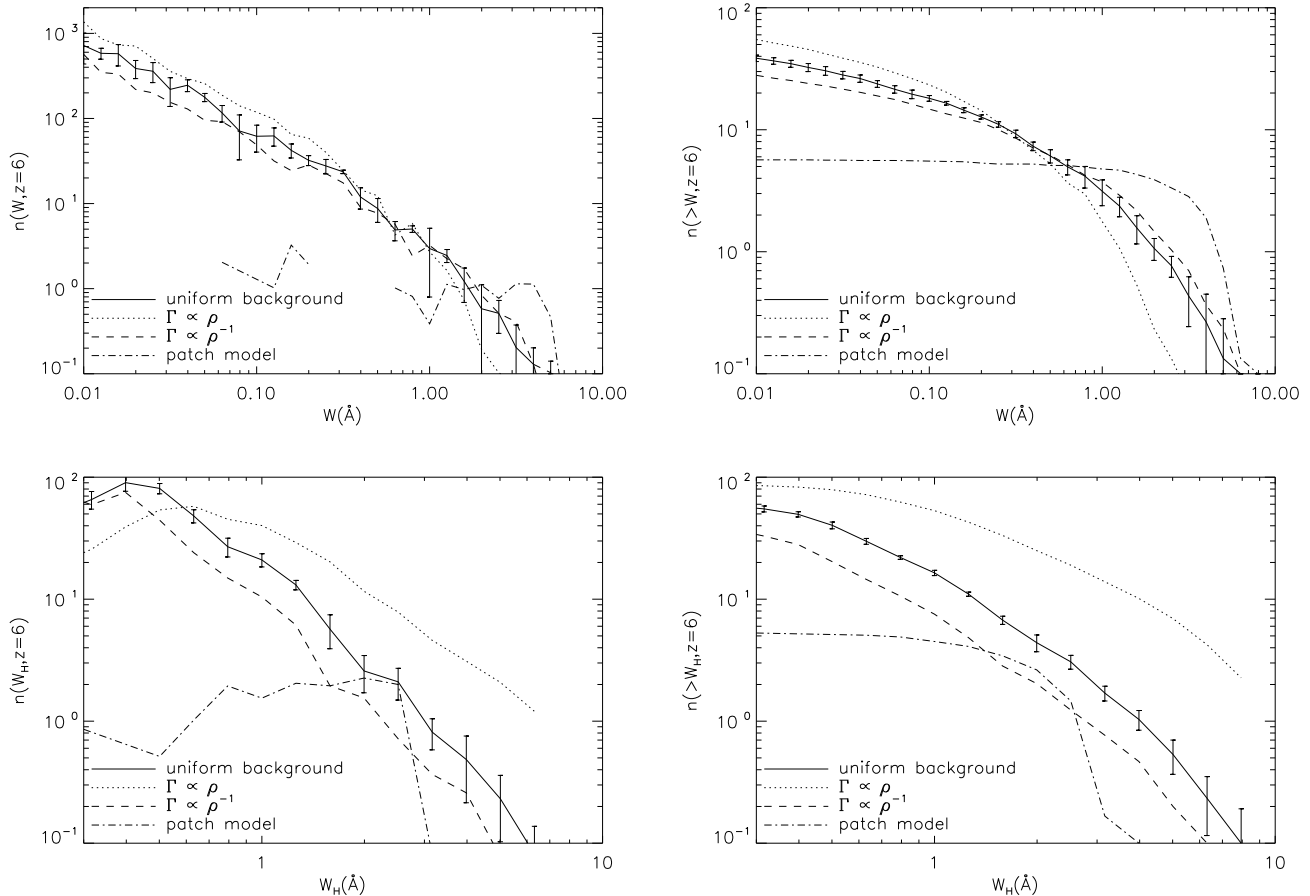


**Figure 10.** Number densities  $n(W, z)$ ,  $n(> W, z)$ ,  $n(W_H, z)$ , and  $n(> W_H, z)$  of leaks for three fluctuating ionizing background models at  $z = 6$ . The error bars of the uniform background model are taken from Figure 5.

## 5 DISCUSSION AND CONCLUSION

We show that the Ly $\alpha$  absorption spectra of UV photon emitters at redshifts around  $z \sim 6$  can be decomposed into Ly $\alpha$  leaks, which come from either lowest density voids or ionized patches containing ionizing sources. The Ly $\alpha$  leaks are well defined and described by the equivalent width  $W$  and the width of half area  $W_H$ . Since both  $W$  and  $W_H$  are defined through integrated quantities, the distributions of Ly $\alpha$  leaks in terms of  $W$  and  $W_H$  are stable with respect to observational noises and instrumental resolution. Although the number densities  $n(W, z)$ ,  $n(> W, z)$ ,  $n(W_H, z)$ , and  $n(> W_H, z)$  evolve very rapidly at redshift  $z \simeq 6$ , these statistics are measurable up to  $z = 6.5$ .

If the Ly $\alpha$  leaks come from lowest density voids, the IGM should be still highly ionized and the ionizing background is almost uniform; in contrast, if the leaks come from isolated ionized patches, the ionizing background should be inhomogeneous, and the reionization is still in the overlapping stage. Therefore, the origin of Ly $\alpha$  leaks is crucial to understand the history of reionization.

We show that the statistics with  $W$  and  $W_H$  are sensitive to the origin of Ly $\alpha$  leaks, because the Ly $\alpha$  leaks are sensitive to the correlation between photon and density fields. Based on physical consideration of reionization, we studied four phenomenological models of the photon field: the

uniform ionizing background (model 0), the photoionization rate  $\Gamma_{\text{HI}}$  is proportional to the density  $\rho$  (model I),  $\Gamma_{\text{HI}}$  and  $\rho$  are anti-correlated (model II), and ionized regions only given by Stromgren sphere around ionizing photo sources (patch model). We found that, although all the four models can fit the observed mean and variance of optical depth at  $z \simeq 6$ , the width distribution of Ly $\alpha$  leaks show very different behaviors.

For model 0, I, and II, most of Ly $\alpha$  leaks are from lowest density voids, and the distribution of dark gaps are similar. However, the properties of individual Ly $\alpha$  leaks are different. Model I gives broader width  $W_H$  than model 0; model II gives narrower width  $W_H$  than model 0. For patch model, the Ly $\alpha$  leaks are mainly from ionized sphere, and they generally have higher maximum of transmitted flux than other models. There is a bump in the distribution of the equivalent width  $W$ , which characterize the intensity of UV photons within ionized patches. Ly $\alpha$  leaks from ionized patches will provide the information of ionized patches, such as their intensity and size, and constrain the properties of UV sources that contribute most of ionizing photons of the reionization.

Finally, we point out that similar analysis is also applicable to the reionization of HeII. The optical depth of HeII Ly $\alpha$  evolves rapidly at  $z \simeq 2 - 3$ . It reaches  $\simeq 5$  at  $z \simeq 3$ . That is, the evolution of HeII reionization at  $z \simeq 3$  would

be similar to that of H at  $z \simeq 6$ . Observed sample of HeII Ly $\alpha$  absorption indeed show structures similar to the leaks of hydrogen absorption spectrum (Zheng et al. 2004). One can also draw the information of background photons at the energy band of HeII ionization.

## ACKNOWLEDGEMENT

This work is supported in part by the US NSF under the grant AST-0507340. LLF acknowledges support from the National Science Foundation of China (NSFC).

## REFERENCES

- Bahcall N.A., Cen R., Davé R., Ostriker J.P., Yu Q., 2000, ApJ, 541, 1
- Bechtold, J. 1994, ApJS, 91, 1
- Becker, G. D., Rauch, M. & Sargent, W. L. W. 2006, astro-ph/0607633
- Berera, A. & Fang, L. Z. 1994, Phys. Rev. Lett., 72, 458
- Bi, H.G. & Davidsen, A. F. 1997, ApJ, 479, 523.
- Bi, H.G., Ge, J. & Fang, L.Z. 1995, ApJ, 452, 90
- Bi, H.G., Fang, L.Z., Feng, L.L. & Jing, Y.P. 2003, ApJ, 598, 1
- Bolton, J. S., Haehnelt, M. G., Viel, M., Springel, V. 2005, MNRAS, 357, 1178
- Bouwens, R. J., Illingworth, G. D., Blakeslee, J. P., Franx, M. 2006, ApJ, 653, 53
- Choudhury, T.R., Srianand, R. & Padmanabhan T., 2001, ApJ, 559, 29
- Choudhury, T.R. & Ferrara, A. 2005, MNRAS, 351, 577
- Ciardi, B., Stoehr, F. & White, S. D. M. 2003, MNRAS, 343, 1101
- Croft, R. A. C. et al. 2002, ApJ, 581, 20
- Ellis, R. S. 2007, astro-ph/0701024, First Light in Universe, Saas-Fee Advanced Course 36, Swiss Soc. Astrophys. Astron
- Fan, X. et al. 2002, AJ, 123, 1247
- Fan, X. et al. 2006, AJ, 132, 117
- Furlanetto, S., Hernquist, L. & Zaldarriaga, M. 2004, MNRAS, 354, 675
- Furlanetto, S. & Oh, S. P. 2005, MNRAS, 363, 1031
- Gallerani, S., Choudhury, T.R. & Ferrara, A. 2006, MNRAS, 370, 1401
- Gallerani, S., Ferrara, A., Fan, X. & Choudhury, T.R. 2007, arXiv:0706.1053.
- Gnedin, N. 2004 ApJ, 610, 9
- He, P., Feng, L.L. & Fang, L.Z. 2004, ApJ, 612, 14
- He, P., Feng, L. L., Shu, C. W. & Fang, L. Z. 2006, Phys. Rev. Lett. 96, 051302
- Haiman, Z. 2002, ApJ, 576, L1
- Hui, L. & Gnedin, N.Y. 1997 MNRAS, 292, 27
- Jena, T. et al. 2005, MNRAS, 361, 70
- Jones, B.T. 1999, MNRAS, 307, 376
- Kohler, K., Gnedin, N. Y., & Hamilton, A. J. S. 2007, ApJ, 657, 15
- Lidz, A., Oh, S. P. & Furlanetto, R. 2006, ApJ, 639, L47
- Liu, J., Bi, H., Feng, L.-L. & Fang, L.-Z. 2006, ApJ, 645, L1 (PaperI)
- Liu, J.R. & Fang, L.Z. 2007, arXiv:0707.2620, ApJ, in press
- Mellema, G., Iliiev, I. T., Pen, U.-L., Shapiro, P. R. 2006, MNRAS, 372, 679
- Miralda-Escude, J. 1998, ApJ, 501, 15
- Miralda-Escude, J., Haehnelt, M. & Rees, M. J. 2000, ApJ, 530, 1
- Oh, S.P., & Furlanetto, S. R. 2005, ApJ, 620, L9
- Page, L. 2007, ApJS, 170, 335.
- Pando, J., Feng, L. L., Jamkhedkar, P., Zheng, W., Kirkman, D., Tytler, D. & Fang, L. Z. 2002, ApJ, 574, 575
- Paschos, P., & Norman, M. L., 2005, ApJ, 631, 59
- Qiu, J.M., Shu, Q.W., Feng, L.L. & Fang, L.Z. 2006, in preparation
- Rauch, M. et al. 1997, ApJ, 489, 7
- Rauch, M. 1998, ARA&A, 36, 267
- Razoumov, A. O., Norman, M. L., Abel, T., & Scott, D., 2002, ApJ, 572, 695
- Seljak, U. et al. 2005, PhRvD, 71, 103515
- Shapiro, P. R., Iliiev, I. T., Alvarez, M. A., Scannapieco, E. 2006, ApJ, 648, 922
- Sokasian, A, Abel, T., Hernquist, L, Springel, V. 2003, MNRAS, 344, 607S
- Songaila, A. & Cowie, L. 2002, AJ, 123, 2183
- Viel, M., Matarrese, S., Mo H.J., Haehnelt, M.G., Theuns, T., 2002, MNRAS, 329, 848
- Viel, M., S., Haehnelt, M.G., Lewis, A. 2006, MNRAS, 370, L51
- Wyithe, J, S. B., & Loeb, A. 2005, ApJ, 625, 1
- Yang, X. H., Feng, L. L., Chu, Y. Q. & Fang, L. Z. 2001, ApJ, 560, 549
- Zheng, W. et al. 2004, ApJ, 605, 631